Time-domain analysis of second-harmonic generation of primary Lamb wave propagation in an elastic plate*

Deng Ming-Xi(邓明晰)[a)†] and Xiang Yan-Xun(项延训)[b)]

[a)] *Department of Physics, Logistics Engineering University, Chongqing* 401331, *China*

[b)] *School of Mechanical and Power Engineering, East China University of Science and Technology, Shanghai* 200237, *China*

(Received 31 March 2010; revised manuscript received 25 April 2010)

Within the second-order perturbation approximation, this paper investigates the physical process of generation of the time-domain second harmonic by a primary Lamb wave waveform in an elastic plate. The present work is performed based on the preconditions that the phase velocity matching is satisfied and that the transfer of energy from the primary Lamb wave to the double frequency Lamb wave is not zero. It investigates the influences of the difference between the group velocities of the primary Lamb wave and the double frequency Lamb wave, the propagation distance and the duration of the primary Lamb wave waveform on the envelope shape of the time-domain second harmonic. It finds that the maximum magnitude of the envelope of the second-harmonic waveform can grow within some propagation distance even if the condition of group velocity matching is not satisfied. Our analyses also indicate that the maximum magnitude of the envelope of the second-harmonic waveform is kept constant beyond a specific propagation distance. Furthermore, it concludes that the integration amplitude of the time-domain second-harmonic waveform always grows with propagation distance within the second-order perturbation. The present research yields new physical insight not previously available into the effect of generation of the time-domain second harmonic by propagation of a primary Lamb wave waveform.

Keywords: Lamb wave, second-harmonic generation, group velocity matching, phase velocity matching

PACC: 4325, 4320, 4335

1. Introduction

In the past few decades, there has been a growing awareness that the elastic nonlinearity of engineering materials can be a very sensitive indicator of some defect states which are difficult to be detected by other means.[1−4] Because Lamb waves are a very important means of nondestructive evaluation of plate-like structures,[5] and the second harmonic in conjunction with primary Lamb wave propagation can include more accurate information about the elastic plates,[6−11] it is essential to study the generation of the second harmonic of primary Lamb wave propagation. However, due to the dispersion and multi-mode of primary Lamb wave propagation, the process of generation of the second harmonic is very complicated. In recent years, some theoretical and experimental studies have been performed on this issue.[12−18] It was found that, under certain conditions, the second harmonic of the primary Lamb wave propagation has a strong nonlinearity, i.e. its amplitude can grow with propagation distance. Recently, some studies focus on using the effect of second-harmonic generation by primary Lamb wave propagation to assess damage in elastic plates.[7,9,10] Experimental results indicate that nonlinear Lamb waves may offer a potential for accurately assessing the early stages of damage in plate-like structures. For observing clear second-harmonic signals by propagation of a primary Lamb wave waveform in the time domain, the corresponding condition for generation of the cumulative time-domain second harmonic must be carefully considered in advance. For the case that the duration of primary Lamb wave waveform in the time domain is infinite, the condition for generation of the cumulative second harmonic requires that the phase velocity matching between the primary and the double frequency Lamb wave (DFLW) modes is satisfied, and that the transfer of energy from the primary Lamb wave propagation to the DFLW component is not zero.[13−16] However, it should be noted that, in practical measurements, the primary Lamb wave waveform with a finite duration in the time domain is commonly used. Even though the phase velocity of primary Lamb wave propagation (de-

*Project supported by the National Natural Science Foundation of China (Grant No 10974256).

†Corresponding author. E-mail: dengmx65@yahoo.com

© 2010 Chinese Physics Society and IOP Publishing Ltd

noted by $c_{\rm P}^{[f]}$) is equal to that of the DFLW (denoted by $c_{\rm P}^{[2f]}$), the group velocity of a primary Lamb wave waveform (denoted by $c_{\rm g}^{[f]}$) is not necessarily equal to that of the DFLW waveform generated (denoted by $c_{\rm g}^{[2f]}$). The published studies indicated that, besides the condition of phase velocity matching (namely $c_{\rm P}^{[f]} = c_{\rm P}^{[2f]}$), the condition of group velocity matching (namely $c_{\rm g}^{[f]} = c_{\rm g}^{[2f]}$) is also strongly recommended when a time-frequency representation (TFR) is used to extract the second-harmonic signal from a Lamb wave waveform propagating in elastic plates.[8−11] Actually, in practical measurements, this requirement is too rigorous due to the dispersion of Lamb wave propagation by nature. For the case that the duration of primary Lamb wave waveform is infinite, the influence of difference between $c_{\rm P}^{[f]}$ and $c_{\rm P}^{[2f]}$ on generation of the cumulative second harmonic has been investigated.[15] What will happen if the condition $c_{\rm g}^{[f]} = c_{\rm g}^{[2f]}$ is not strictly satisfied when $c_{\rm P}^{[f]}$ is equal to $c_{\rm P}^{[2f]}$? It is of significance for practical measurements to analyse the influence of difference between $c_{\rm g}^{[f]}$ and $c_{\rm g}^{[2f]}$ on the generation of cumulative second harmonic by propagation of a primary Lamb wave waveform in the time domain. This paper reports a study focused on this issue.

2. Theoretical fundamentals

Without loss of generality, only the case in which a primary Lamb wave waveform propagates in a single elastic plate will be investigated. For simplicity, we assume that the material of the elastic plate is isotropic and homogeneous with no attenuation and no dispersion, and that the nonlinear effect is sufficiently small that the primary wave amplitude may be taken to be constant in spite of harmonic generation. It is known that, within the second-order perturbation approximation, the second-harmonic field of a primary Lamb wave mode in a single elastic plate can be expanded as a series of symmetric DFLW components using a modal analysis approach.[14,15] Thus, the corresponding second-harmonic field is symmetrical, regardless of whether the primary Lamb wave mode is symmetrical or antisymmetrical.

Figure 1 shows the dispersion curves for a primary Lamb wave (the symmetric S_2 mode) and the symmetric DFLWs propagating in a $2d$ thick aluminum sheet. At the driving frequency given by the vertical dotted line V, a series of symmetric DFLW components (denoted by the points P, P_1, P_2, and P_3, etc) will be generated by the primary Lamb wave (S_2 mode). It is found that the phase velocity of the primary S_2 mode (namely $c_{\rm P}^{[f]}$) is equal to that of the P DFLW component (namely $c_{\rm P}^{[2f]}$). This means that the amplitude of the P DFLW component will grow with propagation distance.[15] Due to the fact that $c_{\rm P}^{[f]}$ is observably different from that of the other DFLW components (denoted by the points P_1, P_2, and P_3, etc in Fig. 1), the contribution of these DFLW components to the second-harmonic field of the primary S_2 mode can be neglected.[15] When the condition $c_{\rm P}^{[f]} = c_{\rm P}^{[2f]}$ is satisfied, the P DFLW component plays a dominant role in the second-harmonic field of the primary S_2 mode. Thus we can only consider the P DFLW component when we analyse the second-harmonic field of the primary S_2 mode at the frequency given by the dotted line V in Fig. 1.

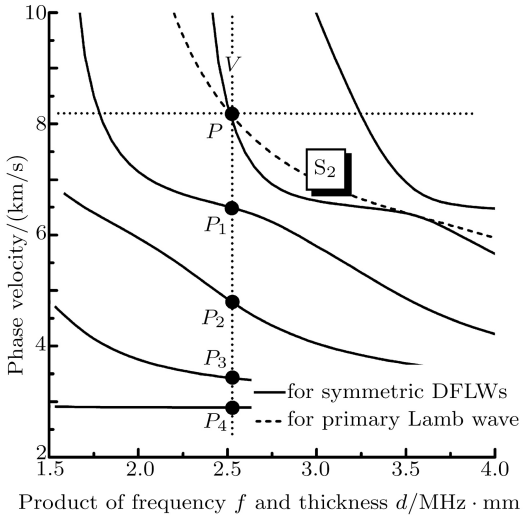


Fig. 1. Dispersion curves for a primary Lamb wave and the symmetric DFLW components.

We consider a time-domain waveform (with the duration τ) of the primary S_2 mode, which is generated at the position T and received at the position R (see Fig. 2). For simplicity, the duration τ of the primary S_2 mode waveform is assumed to be long enough so as to keep its shape unchanged within some propagation distance. This assumption can simplify the process of analysis, and provide a clear physical insight into the complicated problem of the cumulative second-harmonic generation by propagation of a primary Lamb wave waveform in the time domain.

When the time-domain waveform of the primary S_2 mode with the duration τ arrives at the position z_i (here z_i denotes an arbitrary position between T and R in Fig. 2), because of the convective nonlinearity (due to the description difference between

the Lagrangian and Eulerian coordinates) and the inherent nonlinear elastic properties of the solid,[19]

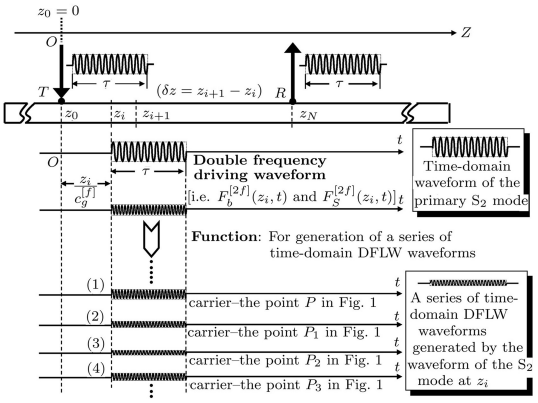


Fig. 2. A series of time-domain DFLW waveforms generated by $F_{\rm b}^{[2f]}(z_i,t)$ and $F_{\rm S}^{[2f]}(z_i,t)$ at z_i. All the DFLW waveforms generated at z_i overlay completely at the moment $t = z_i/c_{\rm g}^{[f]}$, and then they are separated in the time domain due to the different group velocities.

there is a time-domain body driving force of double fundamental frequency (denoted by $F_{\rm b}^{[2f]}(z_i,t)$) in the interior of the isotropic plate, and a time-domain traction stress of double fundamental frequency (denoted by $F_{\rm S}^{[2f]}(z_i,t)$) at the two surfaces of the isotropic plate.[15,16] It is obvious that the duration both of $F_{\rm b}^{[2f]}(z_i,t)$ and of $F_{\rm S}^{[2f]}(z_i,t)$ should be equal to that of the time-domain waveform of the primary S_2 mode, because both the frequency-domain amplitudes of $F_{\rm b}^{[2f]}(z_i,t)$ and $F_{\rm S}^{[2f]}(z_i,t)$ are proportional to the square of frequency-domain displacement amplitude of the primary time-domain waveform.[19] Based on a modal analysis approach, the function both of $F_{\rm b}^{[2f]}(z_i,t)$ and of $F_{\rm S}^{[2f]}(z_i,t)$ is to generate a series of time-domain DFLW waveforms with the duration τ, where the carriers of these time-domain waveforms are, respectively, the DFLW components determined by the points P, P_1, P_2, and P_3, etc in Fig. 1.

At the moment that the primary S_2 mode waveform arrives at z_i and then the corresponding double frequency driving waveform (i.e., $F_{\rm b}^{[2f]}(z_i,t)$ and $F_{\rm S}^{[2f]}(z_i,t)$) occurs, the DFLW waveforms with the duration τ, generated by $F_{\rm b}^{[2f]}(z_i,t)$ and $F_{\rm S}^{[2f]}(z_i,t)$, overlap completely at the time $t = z_i \Big/ c_{\rm g}^{[f]}$ as illustrated in Fig. 2, where the scales (or amplitudes) of the waveforms of the S_2 mode and the DFLWs are only schematic, and do not denote the absolute magnitude. Afterwards, the wave envelopes (or wave packets) of these DFLW waveforms will separate in the time domain because their carriers (i.e. the DFLW components determined by the points P, P_1, P_2, and P_3, etc in Fig. 1) have the different group velocity. Due to the assumption that the duration τ is long enough, the shape of each DFLW waveform can be regarded as unchanged within some propagation distance. When the primary S_2 mode waveform arrives at the position z_{i+1} adjacent to z_i (see Fig. 2), a similar physical process for generation of the DFLW waveforms will take place as described above. Analogically, the same physical process for generation of the DFLW waveforms will continue as far as the position R in Fig. 2. Apparently, the time-domain second-harmonic waveform by the primary S_2 mode waveform at the position R is equal to the sum of all the DFLW waveforms, which are generated by $F_{\rm b}^{[2f]}(z_i,t)$ and $F_{\rm S}^{[2f]}(z_i,t)$ at each position z_i ($i = 0, 1, \ldots, N$; each position z_i is assumed to be equally spaced) and then linearly travel to the position R.

The carriers of the DFLW waveforms shown in Fig. 2 are a series of DFLW components determined by the points P, P_1, P_2, and P_3, etc in Fig. 1. Except for the DFLW component determined by the point P, the phase velocities of the other DFLW components are different from that of the primary S_2 mode, and they are also not equal to each other. Thus, except for the first time-domain waveform whose carrier is the P DFLW component shown in Fig. 1, all the other DFLW waveforms shown in Fig. 2, which are generated by $F_{\rm b}^{[2f]}(z_i,t)$ and $F_{\rm S}^{[2f]}(z_i,t)$ at each position z_i and then linearly travel to the position R, are not in phase in the time-domain overlapping range at the position R, and the corresponding time-domain superposition is out of phase. Therefore, the resultant outcome of these non-coherent DFLW waveforms at the position R is negligible.[15]

Here we focus on the first DFLW waveform in Fig. 2. All the first DFLW waveforms like that shown in Fig. 2, which are generated at each position z_i and then linearly travel to the position R, may overlap adequately at the position R (so long as the duration τ is long enough), and their carriers are in phase in the overlapping range due to the condition of phase velocity matching (namely $c_{\rm P}^{[f]} = c_{\rm P}^{[2f]}$). Thus the resultant outcome of these coherent DFLW waveforms at the position R should be obvious. For the purpose of effective detection of the second-harmonic signal, only the first DFLW waveform like that shown in Fig. 2, which is generated at each position z_i, plays a dominant role in the time-domain second-harmonic signal at the position R, and the contribution of the other DFLW waveforms (their carriers are respectively

the DFLW components determined by the points P_1, P_2, and P_3, etc in Fig. 1) to the second-harmonic signal is trivial. For simplicity, we can figure that both $F_{\rm b}^{[2f]}(z_i,t)$ and $F_{\rm S}^{[2f]}(z_i,t)$ at each z_i only generate the first DFLW waveform like that shown in Fig. 2, and the second, third, and fourth DFLW waveforms, etc are not considered.

First, we analyse the special case in which both the conditions $c_{\rm P}^{[f]}=c_{\rm P}^{[2f]}$ and $c_{\rm g}^{[f]}=c_{\rm g}^{[2f]}$ are simultaneously satisfied (here, $c_{\rm g}^{[f]}$ and $c_{\rm g}^{[2f]}$ respectively denote the group velocity of the primary S_2 mode and that of the P DFLW component at the frequency given by the vertical dotted line V in Fig. 1). Without loss of generality, the time is set to be zero when the time-domain waveform of the primary S_2 mode just reaches the position T ($z=z_0=0$). Figure 3 schematically illustrates the physical process of generation of the second harmonic by propagation of the primary S_2 mode waveform under the conditions of $c_{\rm P}^{[f]}=c_{\rm P}^{[2f]}$ and $c_{\rm g}^{[f]}=c_{\rm g}^{[2f]}$. When the primary S_2 mode waveform arrives at z_0, the time-of-flight of the DFLW waveform (namely the first time-domain DFLW waveform in Fig. 2; generated by $F_{\rm b}^{[2f]}(z_0,t)$ and $F_{\rm S}^{[2f]}(z_0,t)$ at z_0) from the position T to R is $z\Big/c_{\rm g}^{[2f]}$. Similarly, when the primary S_2 mode waveform arrives at an arbitrary position z_i, the time-of-flight of the DFLW waveform (generated by $F_{\rm b}^{[2f]}(z_i,t)$ and $F_{\rm S}^{[2f]}(z_i,t)$ at z_i) from z_i to the position R is $(z-z_i)/c_{\rm g}^{[2f]}$, plus the time-of-flight $z_i/c_{\rm g}^{[f]}$ the primary S_2 mode waveform spends from z_0 to z_i. Due to the condition $c_{\rm g}^{[f]}=c_{\rm g}^{[2f]}$, all the DFLW waveforms shown in Fig. 3, generated at each z_i and then linearly traveling to the position R, will overlap completely in the time domain. At the position R in Fig. 3, the in-phase superposition (due to $c_{\rm P}^{[f]}=c_{\rm P}^{[2f]}$) of all these overlapping DFLW waveforms (generated at each z_i) yields the total time-domain second-harmonic waveform (denoted by $F_{2f}(t)$). It is known that the amplitude of all these DFLW waveforms (generated at each z_i) is the same (denoted by $A^{[2f]}$; see Fig. 3) because the material of the elastic plate is assumed to be isotropic and homogeneous with no attenuation and no dispersion. Due to the in-phase superposition of all these DFLW waveforms shown in Fig. 3, the scale (or amplitude) of the total time-domain second-harmonic waveform $F_{2f}(t)$ is equal to $N\times A^{[2f]}$, i.e. $A_{\rm max}^{[2f]}=N\times A^{[2f]}$. When δz in Fig. 3 is fixed, there is a relationship $N=z/\delta z$. Therefore, it can be concluded that $A_{\rm max}^{[2f]}$ grows with propagation distance. Clearly, the envelope of the time-domain second-harmonic waveform $F_{2f}(t)$ overlaps completely with that of the primary S_2 mode waveform due to the condition of $c_{\rm g}^{[f]}=c_{\rm g}^{[2f]}$.

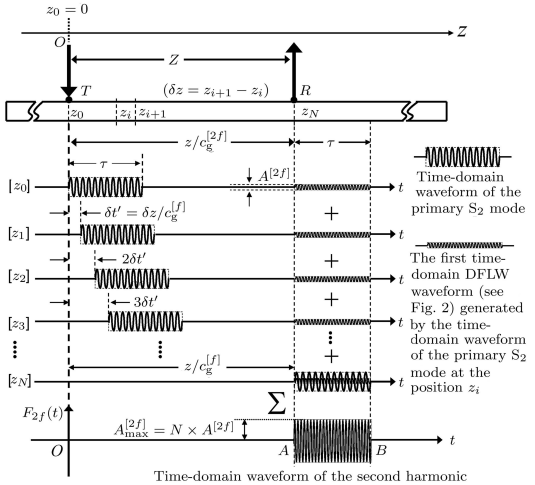


Fig. 3. Physical process of generation of the time-domain second harmonic by the primary S_2 mode waveform under the condition $c_{\rm g}^{[f]}=c_{\rm g}^{[2f]}$.

Next, we investigate the case in which $c_{\rm P}^{[f]}=c_{\rm P}^{[2f]}$ and $c_{\rm g}^{[f]}\neq c_{\rm g}^{[2f]}$. For the P DFLW component at the frequency given by the vertical dotted line V in Fig. 1, we have $c_{\rm P}^{[f]}=c_{\rm P}^{[2f]}$ and $c_{\rm g}^{[f]}>c_{\rm g}^{[2f]}$ ($c_{\rm g}^{[f]}=3.785$ km/s and $c_{\rm g}^{[2f]}=1.960$ km/s). Figure 4 illustrates the physical process of generation of the time-domain second harmonic by the primary S_2 mode waveform under the conditions of $c_{\rm P}^{[f]}=c_{\rm P}^{[2f]}$ and $c_{\rm g}^{[f]}>c_{\rm g}^{[2f]}$. Similar to the analysis process shown in Fig. 3, when the primary S_2 mode waveform arrives at z_0, the time-of-flight of the DFLW waveform (namely the first DFLW waveform in Fig. 2; generated by $F_{\rm b}^{[2f]}(z_0,t)$ and $F_{\rm S}^{[2f]}(z_0,t)$ at z_0) from the position T to R is $z/c_{\rm g}^{[2f]}$. In the same way, when the primary S_2 mode waveform arrives at an arbitrary position z_i, the time-of-flight of the DFLW waveform (generated by $F_{\rm b}^{[2f]}(z_i,t)$ and $F_{\rm S}^{[2f]}(z_i,t)$ at z_i) from z_i to the position R is $(z-z_i)/c_{\rm g}^{[2f]}$, plus the time-of-flight $z_i/c_{\rm g}^{[f]}$ the primary S_2 mode waveform spends from z_0 to z_i. Due to the condition $c_{\rm g}^{[f]}>c_{\rm g}^{[2f]}$, the two DFLW waveforms (being respectively generated at z_0 and z_i, and then linearly traveling to the position R) do not overlap completely. Clearly, at the position R, the time-domain range of the DFLW waveform generated at z_0 is from $z/c_{\rm g}^{[2f]}$ to $[z/c_{\rm g}^{[2f]}+\tau]$, and that of the DFLW waveform generated at z_i is from $[z_i/c_{\rm g}^{[f]}+(z-z_i)/c_{\rm g}^{[2f]}]$ to $[z_i/c_{\rm g}^{[f]}+(z-z_i)/c_{\rm g}^{[2f]}+\tau]$. Figure 4 indicates that, at the position R, the time-domain range of envelope of the second-harmonic waveform is from $z/c_{\rm g}^{[f]}$ to $[z/c_{\rm g}^{[2f]}+\tau]$. Of course, in this range from $z/c_{\rm g}^{[f]}$ to $[z/c_{\rm g}^{[2f]}+\tau]$, all the DFLW waveforms are in phase due to the condition of phase

velocity matching (i.e. $c_{\rm P}^{[f]} = c_{\rm P}^{[2f]}$). Generally speaking, the factors such as the duration of the primary S_2 mode waveform (namely τ), the difference between $c_{\rm g}^{[f]}$ and $c_{\rm g}^{[2f]}$, and the propagation distance z determine the overlapping degree of these DFLW waveforms shown in Fig. 4, and then affect the shape of time-domain envelope of the second harmonic. In the following, we will investigate the influences of these factors on the shape of envelope of the time-domain second-harmonic waveform $F_{2f}(t)$.

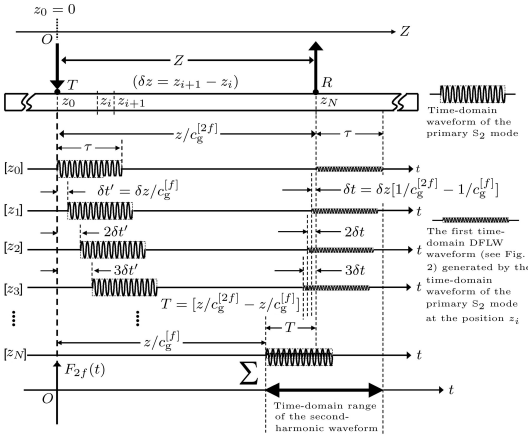


Fig. 4. Physical process of generation of the time-domain second harmonic by the primary S_2 mode waveform under the condition $c_{\rm g}^{[f]} > c_{\rm g}^{[2f]}$.

2.1. Under the condition of $\tau \geq \frac{z}{c_{\rm g}^{[2f]}} - \frac{z}{c_{\rm g}^{[f]}}$

The above condition corresponds to the case where either the propagation distance z (see Fig. 4) or the difference between $c_{\rm g}^{[f]}$ and $c_{\rm g}^{[2f]}$ or both are relatively small. Figure 5 illustrates the physical process of generation of the time-domain second harmonic by the primary S_2 mode waveform under the condition of $\tau > z[1/c_{\rm g}^{[2f]} - 1/c_{\rm g}^{[f]}]$ (namely $T' > 0$). Clearly, the complete overlapping range of all the DFLW waveforms (whose carriers are the P DFLW in Fig. 1), which are generated at each position z_i $(i = 0, 1, \ldots, N)$ and then linearly travel to the position R, is from $z/c_{\rm g}^{[2f]}$ to $z/c_{\rm g}^{[f]} + \tau$ (namely T', or $\overline{BD'}$ or $\overline{B'D}$ in the envelope of the time-domain waveform of the second harmonic; see Fig. 5). In the time-domain range of

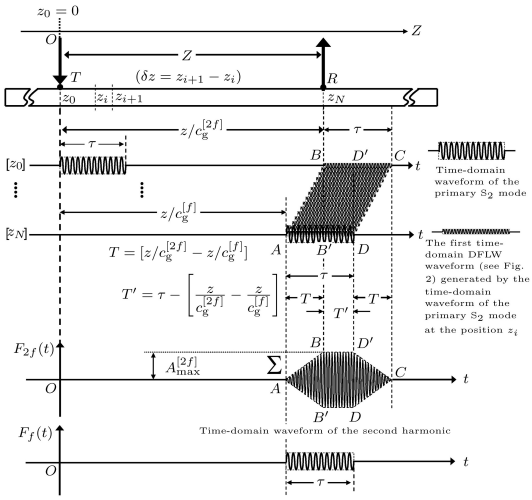


Fig. 5. Physical process of generation of the time-domain second harmonic by the primary S_2 mode waveform under the condition $\tau > z[1/c_{\rm g}^{[2f]} - 1/c_{\rm g}^{[f]}]$.

$\overline{BD'}$ or $\overline{B'D}$, the physical process of generation of the time-domain second-harmonic waveform by the primary S_2 mode waveform is equivalent to that when the duration τ is infinite. Therefore, the amplitude of the second-harmonic waveform in the range of $\overline{BD'}$ or $\overline{B'D}$ is proportional to propagation distance z (namely $A_{\rm max}^{[2f]} \propto z$; see Fig. 3). Both the time-domain waveform of the second harmonic (denoted by $F_{2f}(t)$) and that of the primary S_2 mode (denoted by $F_f(t)$) are schematically illustrated in Fig. 5. In the time-domain range from $z/c_{\rm g}^{[f]}$ to $z/c_{\rm g}^{[2f]}$, the overlapping degree of all the DFLW waveforms, generated at each position z_i $(i = 0, 1, \ldots, N)$ and then linearly traveling to the position R, linearly increases with time as illustrated in Fig. 5, whereas in the range from $z/c_{\rm g}^{[f]} + \tau$ to $z/c_{\rm g}^{[2f]} + \tau$, the overlapping degree of these DFLW waveforms linearly decreases with time. When the position R is fixed (i.e. the propagation distance z is given), the shape of envelope (denoted by $A_{2f}(t)$) of the time-domain second-harmonic waveform $F_{2f}(t)$ can be presented as follows:

$$\begin{cases} A_{2f}(t) = 0, & 0 \leq t < z/c_{\rm g}^{[f]}; \\ A_{2f}(t) = A_{\rm max}^{[2f]} \times (t - z/c_{\rm g}^{[f]})/T, & z/c_{\rm g}^{[f]} \leq t < z/c_{\rm g}^{[2f]}; \\ A_{2f}(t) = A_{\rm max}^{[2f]}, & z/c_{\rm g}^{[2f]} \leq t < z/c_{\rm g}^{[f]} + \tau; \\ A_{2f}(t) = A_{\rm max}^{[2f]} \times (z/c_{\rm g}^{[2f]} + \tau - t)/T, & z/c_{\rm g}^{[f]} + \tau \leq t < z/c_{\rm g}^{[2f]} + \tau; \\ A_{2f}(t) = 0, & t \geq z/c_{\rm g}^{[2f]} + \tau; \end{cases} \quad (1)$$

where $T = z/c_{\rm g}^{[2f]} - z/c_{\rm g}^{[f]}$ is shown in Fig. 5. The envelope $A_{2f}(t)$ is a modulation term, which defines the width, amplitude and shape of $F_{2f}(t)$.

For the case where the duration τ and both $c_{\rm g}^{[f]}$ and $c_{\rm g}^{[2f]}$ are given, the value of T' will approach zero while that of T will approach τ with increase of z until the condition $z = \tau c_{\rm g}^{[f]} c_{\rm g}^{[2f]}/[c_{\rm g}^{[f]} - c_{\rm g}^{[2f]}]$ (namely $\tau = z[1/c_{\rm g}^{[2f]} - 1/c_{\rm g}^{[f]}]$) is satisfied. The corresponding physical process of generation of the time-domain second-harmonic waveform is illustrated in Fig. 6. It is obvious that the magnitude of envelope of the time-domain second-harmonic waveform reaches its maximum at the time $t = z/c_{\rm g}^{[2f]}$ or $t = z/c_{\rm g}^{[f]} + \tau$. At this specified time $t = z/c_{\rm g}^{[2f]}$, all the DFLW waveforms, generated at each position z_i $(i = 0, 1, \ldots, N)$ and then linearly traveling to the position R, overlap completely. So the maximum magnitude of envelope of the time-domain second-harmonic waveform (denoted by $A_{\rm max}^{[2f]}$) is proportional to propagation distance z (namely $A_{\rm max}^{[2f]} \propto z$; see Fig. 3). Similar to Eq. (1), the shape of the envelope $A_{2f}(t)$ of the time-domain second-harmonic waveform $F_{2f}(t)$ can be given by

$$\begin{cases} A_{2f}(t) = 0, \quad 0 \le t < z/c_{\rm g}^{[f]}; \\ A_{2f}(t) = A_{\rm max}^{[2f]} \times (t - z/c_{\rm g}^{[f]})/\tau, \quad z/c_{\rm g}^{[f]} \le t < z/c_{\rm g}^{[2f]}; \\ A_{2f}(t) = A_{\rm max}^{[2f]} \times (z/c_{\rm g}^{[2f]} + \tau - t)/\tau, \quad z/c_{\rm g}^{[2f]} \le t < z/c_{\rm g}^{[2f]} + \tau; \\ A_{2f}(t) = 0, \quad t \ge z/c_{\rm g}^{[2f]} + \tau. \end{cases} \tag{2}$$

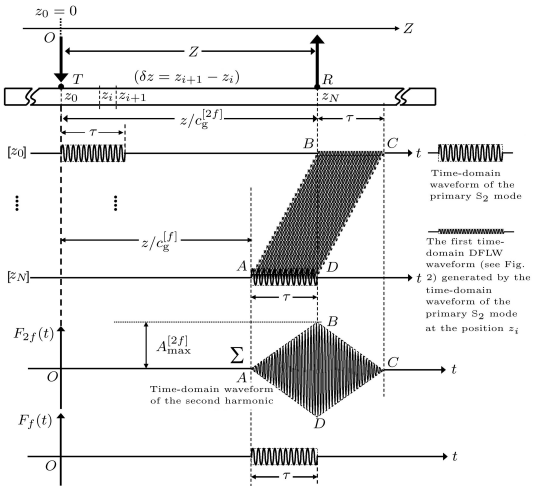


Fig. 6. Physical process of generation of the time-domain second harmonic by the primary S_2 mode waveform under the condition $\tau = z[1/c_{\rm g}^{[2f]} - 1/c_{\rm g}^{[f]}]$.

Based on the modeling shown in Figs. 5 and 6, we can conclude that the maximum magnitude of envelope of the time-domain second-harmonic waveform by the primary Lamb wave waveform grows with propagation distance when the condition $\tau \ge z[1/c_{\rm g}^{[2f]} - 1/c_{\rm g}^{[f]}]$ is satisfied. This result means that the second-harmonic signal by a primary Lamb wave waveform can be clear, even if the condition of group velocity matching is not strictly satisfied.

2.2. Under the condition of $\tau < \frac{z}{c_{\rm g}^{[2f]}} - \frac{z}{c_{\rm g}^{[f]}}$

The above condition corresponds to the case where either the propagation distance z (see Fig. 4) or the difference between $c_{\rm g}^{[f]}$ and $c_{\rm g}^{[2f]}$ or both are relatively large. It also corresponds to the case where the propagation distance z continues to increase beyond the propagation distance $z = \tau c_{\rm g}^{[f]} c_{\rm g}^{[2f]}/[c_{\rm g}^{[f]} - c_{\rm g}^{[2f]}]$ (see Fig. 6). Figure 7 illustrates the physical process of generation of the time-domain second-harmonic waveform $F_{2f}(t)$ by the primary S_2 mode waveform under the condition of $\tau < z[1/c_{\rm g}^{[2f]} - 1/c_{\rm g}^{[f]}]$. Clearly, in the time-domain range from $t = z/c_{\rm g}^{[f]}$ to $t = z/c_{\rm g}^{[f]} + \tau$, the overlapping degree of the DFLW waveforms shown in Fig. 7 linearly increases with time. Thus, the magnitude of the envelope $A_{2f}(t)$ linearly increases with time in the range from $t = z/c_{\rm g}^{[f]}$ to $t = z/c_{\rm g}^{[f]} + \tau$ (namely the slope $\overline{AD}$ in Fig. 7). Then, in the range from $t = z/c_{\rm g}^{[f]} + \tau$ to $t = z/c_{\rm g}^{[2f]}$, the overlapping degree of the DFLW waveforms is kept unchanged. It follows that the magnitude of the envelope $A_{2f}(t)$ is kept constant in the range from $t = z/c_{\rm g}^{[f]} + \tau$ to $t = z/c_{\rm g}^{[2f]}$ (namely $\overline{DB}$ in Fig. 7). Finally, in the range from $t = z/c_{\rm g}^{[2f]}$ to $t = z/c_{\rm g}^{[2f]} + \tau$, the overlapping degree of the DFLW waveforms shown in Fig. 7 linearly decreases with time. Thus, the magnitude of the envelope $A_{2f}(t)$ linearly decreases with time in the range from $t = z/c_{\rm g}^{[2f]}$ to $t = z/c_{\rm g}^{[2f]} + \tau$ (namely the slope $\overline{BC}$ in Fig. 7).

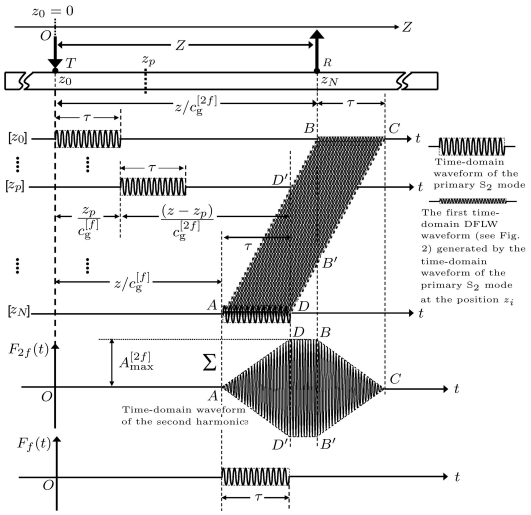


Fig. 7. Physical process of generation of the time-domain second harmonic by the primary S_2 mode waveform under the condition $\tau < z[1/c_{\rm g}^{[2f]} - 1/c_{\rm g}^{[f]}]$.

It should be noted that the duration of envelope with maximum magnitude (denoted by $A_{\max}^{[2f]}$) is in the range from $t = z/c_{\rm g}^{[f]} + \tau$ to $t = z/c_{\rm g}^{[2f]}$, and that $A_{\max}^{[2f]}$ is no longer proportional to the propagation distance z between the positions T and R. Actually, at the position R, the end of the DFLW waveform generated at z_N (namely the point D in Fig. 7) just overlaps with the beginning of the DFLW waveform generated at z_p (namely the point D'). Figure 7 indicates that the DFLW waveforms, generated at each position z_i located between z_p and z_N and then linearly traveling to the position R, completely overlap at $t = z/c_{\rm g}^{[f]} + \tau$. The in-phase superposition of these DFLW waveforms at the specified time $t = z/c_{\rm g}^{[f]} + \tau$ yields the maximum magnitude of the envelope $A_{2f}(t)$. The position z_p can be determined by

$$\frac{z}{c_{\rm g}^{[f]}} + \tau = \frac{z_p}{c_{\rm g}^{[f]}} + \frac{z - z_p}{c_{\rm g}^{[2f]}}, (z = z_N). \tag{3}$$

It follows that $z_p = z - \tau c_{\rm g}^{[f]} c_{\rm g}^{[2f]} / [c_{\rm g}^{[f]} - c_{\rm g}^{[2f]}]$. Similar to the analysis process illustrated in Fig. 3 or 6, $A_{\max}^{[2f]}$ is proportional to the propagation distance between z_p and z_N, i.e. $z - z_p = \tau c_{\rm g}^{[f]} c_{\rm g}^{[2f]} / [c_{\rm g}^{[f]} - c_{\rm g}^{[2f]}]$. Thus, for the case where the parameters such as τ, $c_{\rm g}^{[f]}$ and $c_{\rm g}^{[2f]}$ are given, the maximum magnitude $A_{\max}^{[2f]}$ in Fig. 7 will remain unchanged and independent of the distance z between the positions T and R. Obviously, the duration of the two slopes of the envelope $A_{2f}(t)$ (namely $\overline{AD}$ and $\overline{BC}$ in Fig. 7) is the same, and equal to that of the primary S_2 mode waveform (namely τ). The shape of envelope of the time-domain second-harmonic waveform $F_{2f}(t)$ can be given by

$$\begin{cases} A_{2f}(t) = 0, \quad 0 \le t < z/c_{\rm g}^{[f]}; \\ A_{2f}(t) = A_{\max}^{[2f]} \times (t - z/c_{\rm g}^{[f]})/\tau, \quad z/c_{\rm g}^{[f]} \le t < z/c_{\rm g}^{[f]} + \tau; \\ A_{2f}(t) = A_{\max}^{[2f]}, \quad z/c_{\rm g}^{[f]} + \tau \le t < z/c_{\rm g}^{[2f]}; \\ A_{2f}(t) = A_{\max}^{[2f]} \times (z/c_{\rm g}^{[2f]} + \tau - t)/\tau, \quad z/c_{\rm g}^{[2f]} \le t < z/c_{\rm g}^{[2f]} + \tau; \\ A_{2f}(t) = 0, \quad t \ge z/c_{\rm g}^{[2f]} + \tau. \end{cases} \tag{4}$$

Now, the shape of the envelope $A_{2f}(t)$ has been determined by using the modeling illustrated in Fig. 7. It is found that the maximum magnitude $A_{\max}^{[2f]}$ of the envelope $A_{2f}(t)$ no longer increases with propagation distance. However, it is clear from Eq. (4) that the duration of the envelope $A_{2f}(t)$ with maximum magnitude (namely $\overline{DB}$ in Fig. 7) will increase with increase of propagation distance.

2.3. Influence of propagation distance on the envelope shape of $F_{2f}(t)$

Based on the modeling presented in the above subsections 2.1 and 2.2, the influence of propagation distance on the envelope shape $A_{2f}(t)$ of the time-domain second-harmonic waveform $F_{2f}(t)$ will be investigated for the case where the group velocities (namely $c_{\rm g}^{[f]}$ and $c_{\rm g}^{[2f]}$) and the duration of the primary Lamb wave waveform (namely τ) are given. Similar to the process of analysis illustrated in Figs. 5, 6 and 7, the process of evolution of the envelope shape $A_{2f}(t)$ is illustrated in Fig. 8 for different propagation distance (where $z_a < z_b < z_c < z_d < z_e$). The meaning of the parallelogram $\overline{ABCD}$ in Fig. 8 is exactly the same as that of $\overline{ABCD}$ in Figs. 5, 6 and 7. Clearly, for an arbitrary distance z, the height h of the parallelogram $\overline{ABCD}$ in Fig. 8 is equal to $N \times A^{[2f]}$, where N is equal to $z/\delta z$ and $A^{[2f]}$ is the amplitude of the DFLW waveform (see Fig. 3), which is generated at

each z_i located between the positions T and R and then linearly travels to the position R. When we calculate the height h of the parallelogram $\overline{ABCD}$ in Fig. 8, the duration of all the DFLW waveforms (generated at each z_i located between the positions T and R) can be regarded to be infinite. Thus, the height h of the parallelogram $\overline{ABCD}$ in Fig. 8 is independent of the difference between $c_{\rm g}^{[f]}$ and $c_{\rm g}^{[2f]}$. Clearly from Fig. 8 that the difference between $c_{\rm g}^{[f]}$ and $c_{\rm g}^{[2f]}$ just affects the degree of slope of $\overline{AB}$ or $\overline{DC}$ in the parallelogram $\overline{ABCD}$ when $\delta z = (z_{i+1} - z_i)$ is fixed, and then affects the shape of the envelope $A_{2f}(t)$. The corresponding envelope $A_{2f}(t)$ is presented underneath each parallelogram $\overline{ABCD}$ for different propagation distances. It should be pointed out that z_c is equal to $\tau c_{\rm g}^{[f]} c_{\rm g}^{[2f]} / [c_{\rm g}^{[f]} - c_{\rm g}^{[2f]}]$ (see Fig. 6).

Figure 8 indicates that the maximum magnitude of the envelope $A_{2f}(t)$ increases with propagation distance when z is within z_c, and that it is kept constant when z is beyond z_c. The duration of the envelope $A_{2f}(t)$ with the maximum magnitude (namely $\overline{DB}$ in Fig. 8) will increase with increase of propagation distance under the condition of $z > z_c$. The process of evolution of the envelope shape $A_{2f}(t)$ shown in Fig. 8 is straightforward for different propagation distances. In addition, we should notice the fact that the area of the parallelogram $\overline{ABCD}$ (namely $\tau \times h$) in Fig. 8 is equal to that of the envelope $A_{2f}(t)$ versus time (namely $\int_{t_1}^{t_2} A_{2f}(t){\rm d}t$; $A_{2f}(t)$ is completely located between t_1 and t_2). The integral $\int_{t_1}^{t_2} A_{2f}(t){\rm d}t$ is also known as the integration amplitude of the time-domain second-harmonic waveform $F_{2f}(t)$.[17],1). Thus, the integration amplitude will grow with propagation distance because the area of the parallelogram $\overline{ABCD}$ (namely $\tau N A^{[2f]} = \tau A^{[2f]} z/\delta z$) in Fig. 8 is proportional to propagation distance. This result is independent of the condition of group velocity matching, and it has been verified by the experimental measurements.[17]

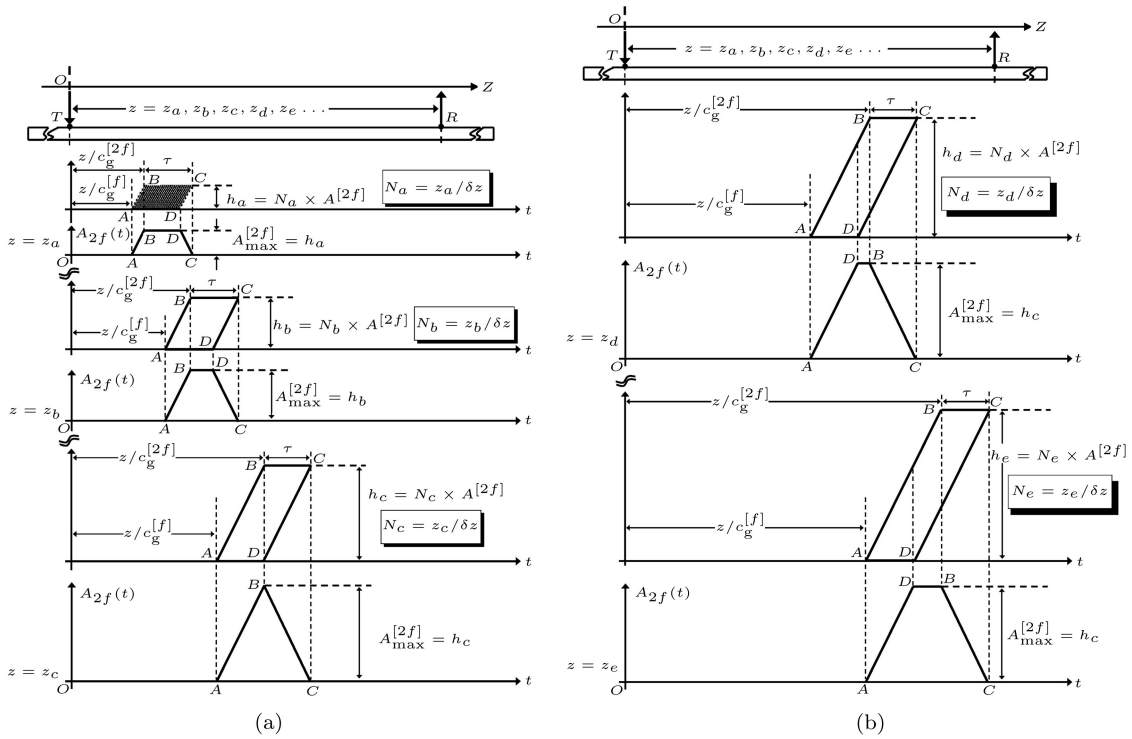


Fig. 8. Evolution process of the envelope shape $A_{2f}(t)$ with increase of propagation distance when the parameters $c_{\rm g}^{[f]}$, $c_{\rm g}^{[2f]}$ and τ are given: (a) $z = z_a$, z_b, and z_c; (b) $z = z_d$ and z_e.

It should be pointed out again that the scale of envelope of the time-domain second-harmonic waveform $F_{2f}(t)$ shown in Figs. 5, 6 and 7 is schematic, and that its absolute magnitude is far less than that of envelope of the primary Lamb wave waveform $F_f(t)$. Moreover, $F_f(t)$ and $F_{2f}(t)$ shown in Figs. 5, 6 and 7 are mixed together in the time domain, and they can be respectively obtained by using the appropriate low-pass and high-pass filters.[6] The present analysis is not concerned with the determination of absolute magnitude of the waveform envelope. Through the present analysis, the physical process of generation of

1) Ritec Advanced Measurement System. Model SNAP-0.25-7 *Operation Manual* RITEC, 2000, USA

the time-domain second harmonic by propagation of a primary Lamb wave waveform has been clearly revealed for the case where the condition of group velocity matching is no longer satisfied. Although some assumptions are made for simplicity, the present analysis yields physical insight not previously available into the process of generation of the cumulative time-domain second harmonic by propagation of a primary Lamb wave waveform in the time domain. We can effectively describe or observe the strong nonlinear effect by propagation of a primary Lamb wave waveform using the envelope function of the time-domain second-harmonic waveform and the corresponding integration amplitude.[17] Of course, if the TFR technique is used to extract the second-harmonic signal from a Lamb wave waveform,[8−11] the rigorous condition of group velocity matching is strongly required.

3. Conclusions

It is of significance for practical measurements to analyse the second-harmonic generation by propagation of a primary Lamb wave waveform with a finite duration. Under the preconditions that the phase velocity matching is satisfied and that the transfer of energy from the primary Lamb wave propagation to the DFLW component is not zero, the analysis of generation of the second harmonic by propagation of a primary Lamb wave waveform in an elastic plate has been performed within the second-order perturbation approximation. For simplifying the process of analysis, it is assumed that the duration of the primary Lamb wave waveform is long enough so as to keep its envelope shape unchanged within some propagation distance. We have investigated the influences of the difference between the group velocities of the primary Lamb wave and the DFLW, the propagation distance and the duration of the primary Lamb wave waveform on the envelope shape of the time-domain second-harmonic waveform. The shape of the envelope of the time-domain second-harmonic waveform has also been formally presented. It is found that the maximum magnitude of the envelope of the second-harmonic waveform can grow within some propagation distance even if the condition of group velocity matching is not satisfied. Our analyses also indicate that the maximum magnitude of the envelope of the second-harmonic waveform is kept constant beyond a specific propagation distance, which depends on the group velocities of the primary Lamb wave and the DFLW, and the duration of the primary Lamb wave waveform. Furthermore, it can be concluded that the integration amplitude of the time-domain second-harmonic waveform always grows with propagation distance within the second-order perturbation. This result is independent of the rigorous condition of group velocity matching, and it is of significance for practical measurements of second-harmonic signals. The present analysis provides a physical insight not previously available into the process of the second-harmonic generation by propagation of a primary Lamb wave waveform in the time domain.

References

[1] Ginsberg J H and Shu K T 1991 *Rev. Prog. Quant. Nondestr. Eval.* **10** B 1829
[2] Nagy P B 1998 *Ultrasonics* **36** 375
[3] Zheng Y P, Maev R G and Solodov I Y 1999 *Canadian J. Phys.* **77** 927
[4] Herrmann J, Kim J Y, Jacobs L J, Qu J M, Littles J W and Savage M F 2006 *J. Appl. Phys.* **99** 124913
[5] Rose J L 2002 *J. Pressure Vessel Technol.* **124** 273
[6] Deng M X 2006 *Ultrasonics* **44** e1157
[7] Deng M X and Pei J F 2007 *Appl. Phys. Lett.* **90** 121902
[8] Bermes C, Kim J Y, Qu J M and Jacobs L J 2007 *Appl. Phys. Lett.* **90** 021901
[9] Pruell C, Kim J Y, Qu J M and Jacobs L J 2007 *Appl. Phys. Lett.* **91** 231911
[10] Pruell C, Kim J Y, Jacobs L J and Qu J M 2009 *Smart Mater. Struct.* **18** 035003
[11] Lee T H and Choi I H 2008 *Mod. Phys. Lett.* B **22** 1135
[12] Deng M X 1999 *J. Appl. Phys.* **85** 3051
[13] Lima W J N 2000 *Harmonic Generation in Isotropic Elastic Waveguides* (Ph.D. Thesis) (The University of Texas at Austin)
[14] Deng M X 2002 *Generation and Propagation of the Second Harmonics of Lamb Waves in Planar Solid Structures* (Ph.D. Thesis) (Shanghai: Tongji University) (in Chinese)
[15] Deng M X 2003 *J. Appl. Phys.* **94** 4152
[16] Lima W J and Hamilton M F 2003 *J. Sound Vib.* **265** 819
[17] Deng M X, Wang P and Lv X F 2005 *J. Phys.* D-*Appl. Phys.* **38** 344
[18] Xiang Y X and Deng M X 2008 *Chin. Phys.* B **17** 4232
[19] Hamilton M F and Blackstock D T 1998 *Nonlinear Acoustics* (New York: Academic) p263